JOURNAL OF MATERIALS SCIENCE **36** (2001) 1331 – 1341

A simplified model for glass dissolution in water

F. DEVREUX,* Ph. BARBOUX, M. FILOCHE, B. SAPOVAL
Laboratoire de Physique de la Matière Condensée, Ecole Polytechnique & CNRS
91128 Palaiseau Cedex, France
E-mail: fd@pmc.polytechnique.fr

Numerical simulations of the water dissolution of a random ternary solid are presented. The three elements represent silica, soluble oxides (alkalis and boron) and quasi-insoluble oxides (Al_2O_3, ZrO_2, Fe_2O_3, . . .). The soluble species are dissolved immediately when they are in contact with the solution. Their proportion is kept below the percolation threshold. For the other species, one introduces a model of dissolution-recondensation. It is shown that the dissolution rate constants should be dependent on the bonding environment in order to include surface tension. The condensation fluxes are proportional to the concentration of each species in solution. In the dynamic regime (no recondensation), one observes the congruent dissolution of silica and soluble species, after a short initial phase of selective extraction of the soluble species. The common rate of dissolution decreases with the proportion of insoluble species and increases sharply with that of soluble species. This is mainly due to the formation of a porous hydrated layer whose active surface area increases markedly with the proportion of soluble species. In the static regime (finite solution volume), the equilibrium solubility of silica decreases with the proportion of insoluble species and is practically independent of the proportion of soluble species. The porous hydrated layer is rearranged and almost free of soluble species. The ripening of the surface layer makes it protective and inhibits further extraction of the soluble species. These results are in general agreement with the experimental observations on the dissolution of durable glasses.

1. Introduction

Glass leaching is an important question in different technological domains. In the field of waste confinement (radioactive or not), it is highly desirable to achieve high glass durability. On the other hand, the glass-fibers used in human environment and liable to be inhaled should be easily dissolved. In any case, the understanding of the corrosion mechanisms is the key point to design glasses with suitable properties. There is a considerable literature, both theoretical and experimental, on the subject [1–31]. A number of important mechanisms have been identified: dissolution of the silica network, interdiffusion of alkalis and hydrogen, formation of a hydrated layer (sometimes called "gel") at the glass-solution interface.

The dissolution behaviour depends on both the glass composition and the leaching solution. These two factors are not independent, since glass alteration modifies the properties of the solution. Particularly, removal of alkalis from the glass increases the solution pH and makes silica more soluble. Hench and Clark have established a classification in five types [5]. Type I, which includes pure silica in neutral pH, corresponds to inert glasses where alteration is limited to the formation of a very thin (∼5 nm) surface hydration layer. Types II and III are durable glasses, which are protected by the formation of hydrated dealkalized layer from a few tens to a few hundreds of nm at their surface. This is observed for glasses with low alkali content in moderate pH conditions (pH < 9). Type III differs from type II by the presence of an extra layer due to the redeposit of secondary phases such as Al_2O_3-SiO_2 or CaO-P_2O_5. In type IV, which corresponds to glasses with high alkali content, the hydration layer is not sufficient to protect the glasses from further dissolution. Finally, type V corresponds to complete and non-selective dissolution. It is observed in high pH situation (pH > 9 ∼ 10).

More recently, Kinoshita *et al*. [19] have studied the dissolution of borosilicate glasses in controlled low pH conditions. They have obtained two classes of behaviour according to the boron proportion in the glass. For high content, the dissolution is congruent, rapid and linear in time. For lower content, they observe selective extraction of boron and sodium with sublinear kinetics for the release of glass elements in solution. They interpret their results in terms of percolation. For high boron content, the silica network is not percolating and the disconnected silica clusters are dragged away together with the soluble species. For lower boron content, the silica network becomes percolating and the soluble components are selectively extracted from the glass.

* Author to whom all correspondence should be addressed.

A number of studies have been devoted to nuclear waste glasses (see ref. [25] for a review). At the very beginning, alkali and boron atoms are released selectively, resulting in the formation of an alkali- and boron-depleted layer. Then, silicon, boron and alkalis are dissolved congruently. Finally, the alteration is stopped or at least strongly slowed down when the solution gets saturated in silica [22, 25]. In this saturation regime, dissolution is non-congruent again with higher release of boron and alkalis [20]. It has been observed that minute changes in glass composition may result in strong differences in the alteration behaviour [15, 23, 24]. In a recent study, the alteration of the reference french nuclear glass R7T7 has been compared to that of simplified glasses with higher alkali contents [30]. While R7T7 is dissolved almost congruently, it has been possible to extract selectively 100% of the boron and alkali atoms contained in some simplified glasses. In the same study, it has been shown by SAXS and thermoporometry techniques that the pores in the hydrated alteration layer are in the 2–4 nm range in diameter. It is highly tempting to interpret these results again within the percolation scheme. In durable glasses, soluble species (mainly boron and alkalis) are below the percolation threshold and can be removed selectively only in the early phase of leaching. Then, the whole dissolution is controlled by that of the main silica network. In non-durable glasses, soluble species can be removed selectively without limit. In turn, this creates a porous hydrated network, which offers a increased active surface area for the dissolution of the silica network.

This leads us to distinguish three dissolution regimes separated by two thresholds. The first threshold would correspond to the percolation of the silica network and the second one to the percolation path for the extraction of soluble species. For silica-poor glasses, the silica content is insufficient for achieving a continuous silica network (i.e., a percolating cluster). Then, the departure of the soluble oxides, either covalently bonded (boron) or disrupting the network (alkalis), produces the complete disintegration of the glass, with the finite silica polymers being released in solution as colloidal particles. In the intermediate regime, both the silica network and the path for the extraction of the soluble oxides are percolating. Thus, it is possible to remove completely the soluble species without disturbing the silica network. In that case, there are two alteration mechanisms in parallel, silica dissolution and soluble oxide extraction. Finally, when the content in soluble oxides is even smaller, the paths for their extraction are no more percolating and their finite clusters are entrangled within the silica matrix. Then, the dissolution of silica is the limiting step of the alteration, including the release of the soluble oxides (as long as one can neglect the diffusion in the solid state). These three regimes have been clearly identified in a Monte Carlo simulation by Aertsens and Van Iseghem [27]. Moreover, it has been shown recently that sublinear leaching kinetics is expected in the neighbouring of the second threshold [32].

In the present paper, we are dealing with the leaching of durable glasses in neutral to moderate basic solutions, with special attention to the problem of nuclear waste glasses. Thus, we keep the proportion of soluble species below the percolation threshold. We also assume that the interdiffusion of alkalis and hydronium in the glass can be neglected. An elementary model is defined for the dissolution-recondensation of silica and the other weakly soluble species. The numerical simulations are worked out both in the far-from-saturation and saturation regimes. A preliminary study restricted to two-dimensional systems has been published recently [33].

Although the model we propose is oversimplified and may appear somewhat naive, it will prove able to reproduce the basic features of the dissolution of durable glasses. Moreover, as shown by recent studies [27, 29, 32–36], numerical simulation provides a convenient way to investigate corrosion dynamics and to visualize corrosion patterns. Both are closely related, since corrosion generates specific morpholologies, but, in turn, morphology changes the course of corrosion. For this reason, we believe that numerical simulations may provide an heuristic approach for a better understanding of the challenging question of the long-term behaviour of nuclear waste glasses.

The correspondence between real glasses and our model glass is discussed in Section 2. Some computational details are given in Section 3. The model for dissolution and recondensation of silica is developed in Section 4. It is shown that surface tension should be included in order to achieve realistic morphologies of the hydration layer. Section 5 is devoted to the stationary dissolution rate in open conditions and Section 6 to the aging in saturation conditions. The effect of the glass surface area to solution volume ratio, which is an important experimental parameter, is emphasized. The influence of less-soluble oxides, such as Al_2O_3 or ZrO_2, is studied in Section 7. The relevance of the model is discussed in Section 8 and the main conclusions are summarized in Section 9.

2. Glass representation

Commercial glasses generally contain several (3 to 10) components. In the case of nuclear waste glasses, there are frequently more than 20 oxides, the major components being SiO_2, B_2O_3, Na_2O, Al_2O_3, Fe_2O_3, CaO, ZrO_2, UO_2 . . . . To simplify, we arrange them into three classes, according to their dissolution behaviour in water. Class A corresponds to the silica matrix, which is the main component of the glass (typically 50 to 60% in nuclear glasses), class B includes the soluble species, mainly the alkali and boron oxides, and finally, class C corresponds to the less soluble oxides, such as Al_2O_3, Fe_2O_3, ZrO_2, rare earth and transuranic oxides. The three species A, B, C in fractions p_A, p_B and p_C are randomly distributed on a tridimensional lattice. At the moment, only the cubic lattice has been studied. Moreover, we have ignored the possible correlations between the positions of the different species, which may result from the clustering of boron and alkalis or from the association of compensating with modifying cations. The oxygen atoms disappear in this simplified representation. However, when we will refer to A-A, A-B or A-C

bonds, it should be understood that these bonds are not direct but involve oxygen atoms as intermediaries.

The correspondence between the composition of a real glass and that of our model glass is not a trivial problem. Since our model emphasizes geometrical aspects related to percolation and since oxygen occupies most of the volume, one can propose to establish this correspondence by counting the oxygen atoms which are associated with each type of cation. However, one should not consider the valence of the cations, but their coordination number. For instance, the tetravalent zirconium is in octahedral environment and the trivalent aluminium is known to be tetrahedral in glasses (although it can be octahedral in other circonstances). This implies that some ionic cations (earth alkalis by preference and alkalis by default) remain in glasses in order to compensate for the negative charges due to the excess oxygen atoms bonded to Zr or Al. Those compensating cations should then be thought as less soluble C species. For example, let us consider a glass whose composition expressed in proportion of oxide moles would be:

$$55\%\ SiO_2,\ 15\%\ B_2O_3,\ 15\%\ Na_2O,\ 5\%\ CaO,$$
$$5\%\ Al_2O_3,\ 5\%\ ZrO_2$$

There are 200 oxygen atoms, of which 110 are associated to Si, 20 to tetrahedral Al and 15 to octahedral Zr, leading to $A:B:C = 55:27.5:17.5$ as the corresponding composition for the model glass. This counting provides a way to classify multicomponent glasses with respect to each others and should allow to compare the predictions of the simulations with experiments when the glass composition is changed.

However, the A : B : C ratios obtained in this way do not constitute an absolute scale. In effect, the site percolation threshold plays a leading role in our model. The threshold is worth 0.3117 for a cubic lattice but changes from one lattice to another [37]. It is *a priori* difficult to assess its value for a real glass, since it has a complicated, disordered and possibly inhomogeneous structure. Moreover, taking into account interdiffusion of alkalis and hydronium ions may change the effective threshold with respect to its static value. Only experiments may solve this problem. Experimental studies on a series of glasses whose composition is gradually changed are currently in progress in our laboratory [38].

3. Computational procedure

Most of the simulations have been performed using an initial free surface area $S = 64 \times 64$ sites. A few simulations have been made with $S = 128 \times 128$ or $S = 256 \times 256$. They do not show differences with respect to those presented below (except for a multiplication of the calculation time by 4 or 16). One elementary computer step includes two successive phases, dissolution and condensation. During the dissolution phase, surface B atoms are dissolved without conditions and surface A and C atoms are removed by random choice according to a model to be defined below (Sections 4 and 7). During the condensation phase, A and C atoms may be deposited again on the surface by random choice with a probability proportional to their concentration in solution. It turns out that it does not matter whether one dissolves B species step-by-step or removes altogether the B clusters connected to the surface, as long as the dissolution of A species is slow enough. To meet this requirement, the highest probability of dissolving a A atom has been kept equal to or less than 0.1, which means that the weakest A atoms have at most 1 chance out of 10 to be removed within a computer step. We have checked that dividing all the probabilities by 10 has no other effect than slowing down the kinetics by a factor of 10 (and multiplying the duration of the simulation by nearly the same factor). Cyclic conditions are imposed in the directions x and y perpendicular to the leaching progress. Accordingly, if the sites $(0, y, z)$ and $(63, y, z)$ are occupied respectively by water and solid species (A, B or C) in a $64 \times 64 \times Z$ simulation, the atom on the site $(63, y, z)$ is considered as belonging to the solid-solution interface and can be dissolved. The same is true for sites $(x, 0, z)$ and $(x, 63, z)$.

Two kinds of experiments have been simulated by choosing the volume V of the leaching solution. Simulations with $V = \infty$ are equivalent to Soxhlet experiments in which continuously replenished water flows on the glass surface. Concentrations in solution are always zero and there is no recondensation of the dissolved species. This makes it possible to determine the initial dissolution rate (Section 5). On the contrary, simulations with a finite volume are equivalent to the so-called static conditions. After some time, the solution gets saturated in A species and one obtains the equilibrium concentration (Section 6). The smaller the solution volume, the shorter the time required to reach saturation. Since this is true in simulations as well as in experiments, most of the simulations have been made with a small volume of $V = 10^9$ solution sites. With $S = 64 \times 64$, this gives a surface area to solution volume ratio $S/V = 4 \times 10^{-6}$, which corresponds to $2 \times 10^4\ m^{-1}$, taking 0.2 nm as the molecular size of water. Such value is easily reached by putting a powdered glass sample in a small container (e.g. 2 g of powder with a specific area of 1 m^2/g in 100 ml of water). It is representative of the high S/V ratios used in some experimental studies [17, 20, 24]. However, a few simulations have also been performed at a smaller S/V, in order to study the effect of this experimental parameter on the glass morphology at saturation.

In simulations with a finite solution volume, it may happen that the pores which have been created by dissolution become closed by the redeposition of A or C atoms. In that case, the simulation should not allow to dissolve into the main solution (the 'ocean') atoms which are on the border of a closed pore (a 'lake'). Also, it may happen that dissolution cuts off aggregates ('islands') from the main solid (the 'continent'). These aggregates, which are the equivalent of colloidal particles, should then be removed in one piece. Taking into account these effects requires the determination of the connectivity of the fluid and that of the solid. As this determination by brute-force method is heavily time-consuming, we have implemented the more sophisticated but much faster algorithm, which was proposed

by Hoshen and Kopelman for the study of percolation clusters [39].

4. Model for dissolution

The standard model for glass dissolution involves interdiffusion of hydronium and alkali ions in parallel with the dissolution of the covalent silica network [2]. The hydrolysis and condensation reactions of Si-O-Si bonds are known to be rather slow, particularly in the zone of interest for the pH that we consider here: $6 < \mathrm{pH} < 9$ [1]. In the case of durable nuclear glasses, it is believed that the dissolution of the silica network is the dominant process, except at very short time and possibly at very long time [10, 16, 22, 25]. Although interdiffusion may play an important role in acidic conditions, it does not seem to control the alteration of glasses by natural water where the pH rises above 7. In most cases, light alkalis and boron are dissolved congruently. As there is no reason for these species to have a similar diffusion coefficient in the glass, this indicates that diffusion is not the controlling step of the dissolution mechanism. Thus, we simply assume that the soluble B species are dissolved immediately if and only if they are at the solid-solution interface, which amounts to suppose that the diffusion is very fast in the hydrated pores of the altered layer and very slow in the solid state. Moreover, the solution volume is supposed to be large enough for the dissolved B species never to condense again at the solid surface.

First-order kinetics is considered to give a good first-approximation description of the dissolution of the silica network [10]. This leads us to write the dissolution rate of the A species as:

$$\frac{\mathrm{d}N_\mathrm{A}}{\mathrm{d}t} = \sum_i [k_\mathrm{d} - k_\mathrm{d} c_\mathrm{A}] \qquad (1)$$

where k_d and k_c are the dissolution and condensation rate constants and c_A is the A concentration in solution (expressed as a molar fraction). In Equation 1, the sum runs over all the sites i of the actual surface. It is often implicitly assumed that the surface area is constant and equal to the initial area before alteration. Let S be this area and V the solution volume. Then, the solution of Equation 1 is:

$$c_\mathrm{A}(t) = c_\mathrm{A}^\mathrm{eq}\left[1 - \exp\left(-\frac{S}{V} k_\mathrm{c} t\right)\right] \qquad (2)$$

with $c_\mathrm{A}^\mathrm{eq} = k_\mathrm{d}/k_\mathrm{c}$ being the equilibrium solubility. Equation 2 implies a scaling of the alteration data with $(S/V) \times t$, which has led experimentalists to use high S/V ratio to investigate the long-term behaviour. In fact, the situation is not so simple. The actual surface area of the altered glass is not equal to the initial area, the $(S/V) \times t$ scaling is not obeyed and Equation 1 misses an essential ingredient -the surface tension- to account for a realistic morphology of the altered glass surface.

Equation 1 has been simulated for an AB system with $p_\mathrm{A} = 0.75$ and $p_\mathrm{B} = 0.25$. As most of the experimental tests on nuclear waste glasses are performed at

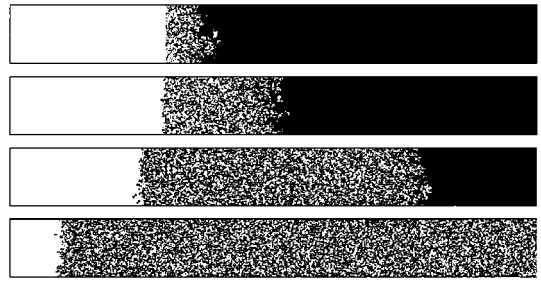

Figure 1 Evolution of a longitudinal cross-section (64×512) in the model described by Equation 1. The parameters of the simulation are: $p_\mathrm{B} = 0.25$, $k_\mathrm{d} = 10^{-3}$, $k_\mathrm{c} = 10$ and $S/V = 4 \times 10^{-6}$. Views at times $t = 10^3$, 3×10^3, 10^4 and 3×10^4.

90°C, where the solubility is typically in the range 50–200 mg/l of Si, $k_\mathrm{d}/k_\mathrm{c}$ was taken equal to 10^{-4} to achieve a realistic solubility (10^{-4} corresponds to 5.5 m mol/l or 150 mg/l of Si). The results are shown in Fig. 1, which displays the time evolution of a 64×512 longitudinal cross-section of the sample (this corresponds to about 20×512 mm^2 taking 0.3 nm as a typical size for the sites in glass). One sees that the whole sample is progressively changed into a swollen foam. As a consequense, the leaching front progresses endlessly inside the sample and B species are extracted continuously at a rate close to the initial rate. It should be mentionned that the transformation into foam is also observed for $p_\mathrm{A} = 1$ (pure silica). The reason for this behaviour is easy to understand: since surface A species are dissolved without consideration for their bonding environment, there is no surface tension and thus no enthalpic forces to fight against entropy, for which a foam is much more favorable than a monolithic sample. For $p_\mathrm{A} < 1$, this low-density foam allows soluble species to be extracted without limit. Although such a behaviour may be observed in a highly aggressive alkaline leachant, it is not expected to occur under moderate pH conditions (pH $\approx$ 6 to 9) which are the realistic ones for nuclear glasses in a disposal environment.

The simplest way to introduce surface tension consists in making the dissolution rate constant dependent on the environment of the A atom to be dissolved. To this end, one introduces the rate constants for hydrolysis (w_h) and condensation (w_c) of one single A-A bond (this A-A bond actually represents the siloxane bond Si-O-Si). The (relative) stability of the glass causes the ratio $\delta = w_\mathrm{h}/w_\mathrm{c}$ to be smaller than 1. Then, the dissolution rate $w_\mathrm{d}(i)$ of an A atom on a surface site i depends on its number of A neighbours n_i as:

$$w_\mathrm{d}(i) = n_i w_\mathrm{h} \left(\frac{w_\mathrm{h}}{w_\mathrm{c}}\right)^{n_i - 1} = n_i w_\mathrm{c} \delta^{n_i} \qquad (3)$$

In this expression, $(w_\mathrm{h}/w_\mathrm{c})^{n_i - 1}$ is the probability that all bonds but one are broken at a given time, n_i stands for the number of ways to choose these $n_i - 1$ bonds, and w_h is the probability (per time unit) of breaking the last one. This formulation implies that the energy of the A-B bonds (actually Si-O-B or Si-O-Na) is negligible, in agreement with the hypothesis of immediate dissolution of B species. As A atoms are dissolved, their concentration in solution increases and they may

be deposited again on surface site i with a rate constant given by:

$$w_r(i) = n_i w_c c_A \quad (4)$$

where n_i stands for the number of possible connections at site i and w_c for the probability of forming a bond (per time unit). Equation 4 assumes that once a A-A bond has been established, the other $n_i - 1$ bonds are formed before the initial one is broken. It is also assumed that the dissolved atoms are uniformly distributed, since diffusion is considered to be fast in the solution. Within this model, the kinetic equation becomes:

$$\frac{dN_A}{dt} = \sum_i [w_d(i) - w_r(i)] = w_c \sum_i n_i \left[\delta^{n_i} - c_A\right] \quad (5)$$

As one of the rate constants (either w_h or w_c) is arbitrary (it gives the time scale of the simulation), AB systems are simply described by two dimensionless parameters, p_B and δ, which characterize the glass composition and silica-water chemistry, respectively. The model will be generalized in Section 7 to include less soluble C species. Since Equation 3 can be interpreted energetically by taking $\delta \sim \exp(-E/k_B T)$, where E would be the energy of a single A-A bond, our model for dissolution is equivalent to that used by Aertsens and Van Iseghem [27, 29], except for the prefactor n_i. Actually, this prefactor is not very important. A few simulations have been made by dropping it from Equations 3–5. Their results are not qualitatively different from those presented below.

5. Dissolution rate

In this section, we describe the results of simulations without recondensation of A species. Fig. 2 shows the evolution of a longitudinal cross-section (64×512 sites) in two simulations with the same kinetics constant ($\delta \equiv w_h/w_c = 0.05$), but with two different glass compositions ($p_B = 0.15$ and $p_B = 0.20$). The subsequent pictures are separated by 5×10^4 time steps in the first experiment and by 10^4 steps in the second one. The leaching front moves forward linearly in time, but much faster for $p_B = 0.20$ than for $p_B = 0.15$. One also observes the existence of a porous layer at the interface between the solid and the solution whose thickness remains constant in time. This layer becomes thicker as p_B is changed from 0.15 to 0.20. Fig. 3 displays the time evolution of the ratio of the current area to the initial area for different values of p_B. After a transient, the area of the porosified interface gets stabilized at a stationary value, herafter denoted as S_0. It turns out that this stationary surface area increases steeply with p_B, which reflects the increasing thickness of the porous layer shown in Fig. 2.

Fig. 4 displays the variation with time of z_f, the position of the front, and that of $n_A = N_A/S$ and $n_B = N_B/S$, the numbers of A and B atoms dissolved per (initial) surface unit for $p_B = 0.25$. At the beginning, there is a phase of non-stochiometric dissolution, which corresponds to the selective extraction of the B clusters connected to the initial interface. The kinetics of dissolution

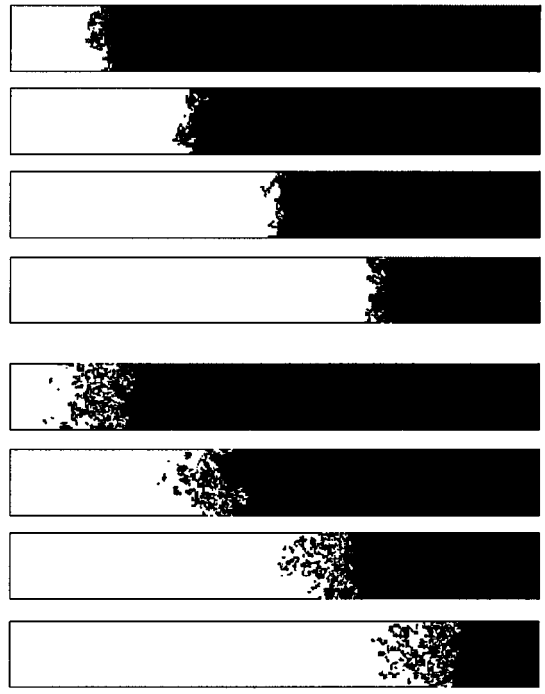

Figure 2 Evolution of a longitudinal cross-section (64×512) in two simulations without recondensation of A species ($V = \infty$). The hydrolysis and condensation rates are the same in both cases: $w_h = 0.1$ and $w_c = 2$ ($\delta \equiv w_h/w_c = 0.05$). Top: $p_B = 0.15$ and $t = 5 \times 10^4$, 10×10^4, 15×10^4 and 20×10^4. Bottom: $p_B = 0.20$ and $t = 1 \times 10^4$, 2×10^4, 3×10^4 and 4×10^4.

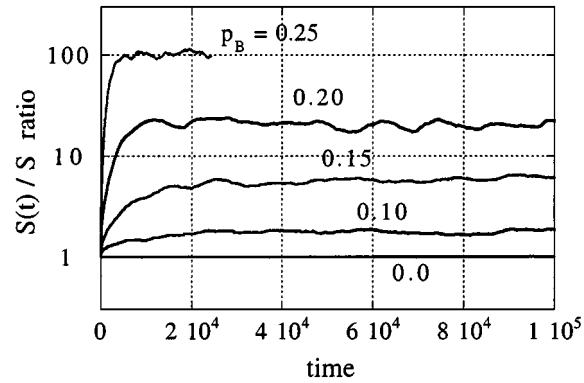

Figure 3 Variation with time of the ratio $S(t)/S$ of the area of the porous network to the initial area ($w_h = 0.1$, $\delta = 0.05$ and $V = \infty$). From bottom to top: $p_B = 0.0$, 0.10, 0.15, 0.20 and 0.25.

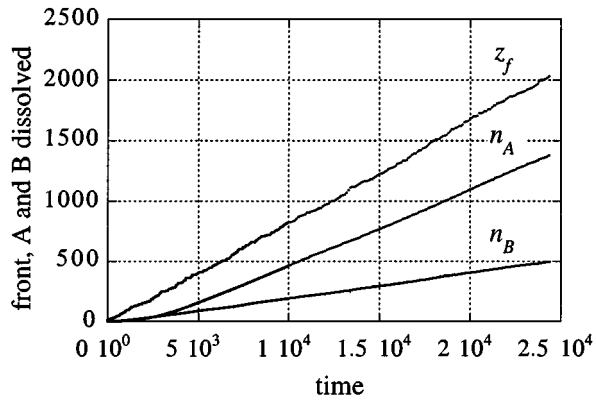

Figure 4 Variation with time of the position of the front, z_f, and of the amounts of dissolved A and B atoms per initial surface area unit, $n_A = N_A/S$ and $n_B = N_B/S$. The parameters of the simulation are: $p_B = 0.25$, $w_h = 0.1$, $\delta = 0.05$ and $V = \infty$.

in this initial phase should be controlled either by the diffusion or the dissolution of the soluble species. It is not properly described within our model, which neglects interdiffusion and assumes instantaneous dissolution of the soluble species at the solid-liquid interface. After this transient, z_f, n_A and n_B increase linearly in time. If one defines rates as:

$$v_f = \frac{dz_f}{dt} \qquad v_A = \frac{dn_A}{dt} \qquad v_B = \frac{dn_B}{dt} \tag{6}$$

it turns out that they obey the relation:

$$v_f = \frac{v_A}{p_A} = \frac{v_B}{p_B} \equiv v_0 \tag{7}$$

for all the values of the parameters p_B and δ we have studied. This means that the dissolution is congruent and controlled by the dissolution of A species. The common value of v_f, v_A/p_A and v_B/p_B is the stationary rate of dissolution v_0, which should be understood as the mean number of single layers dissolved per calculation step. Comparing the simulation result for v_0 with the experimental dissolution rates should make it possible to set the value of a computer step in real time unit.

Fig. 5 displays the main result of this section, i.e. the variation of the dissolution rate v_0 with the parameters p_B and δ. It appears that v_0 depends markedly on both parameters. Especially, it increases more than exponentially with the proportion of soluble B species. This result is in full agreement with experimental data. For example, Bunker *et al*. have shown that the dissolution rate increases by three orders of magnitude from pure silica to the borosilicate glass $(SiO_2)_{0.70}$ $(Na_2O)_{0.15}$ $(B_2O_3)_{0.15}$ [12]. In fact, v_0 is expected to diverge when the proportion of B atoms in the glass approaches the percolation threshold, since the surface of the porous network available for the dissolution of A atoms should increase in huge proportions. However, an accurate description of the dissolution near the threshold would require to introduce a limitation in the rates of dissolution and/or diffusion of the B species.

The variation of the rate of dissolution can be rationalized by expressing v_0 from Equations 5–7 as:

$$v_0 \equiv \frac{1}{p_A S}\frac{dN_A}{dt}\bigg|_0 = \frac{w_c}{p_A}\frac{S_0}{S}\langle n_i \delta^{n_i}\rangle_{i\in S_0} \tag{8}$$

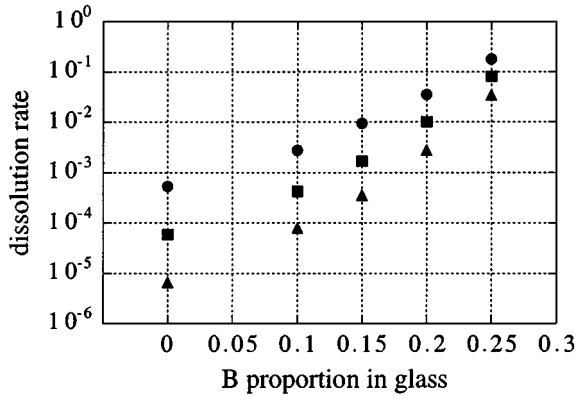

Figure 5 Variation of the dissolution rate v_0 as a function of the proportion p_B of soluble species in glass for $\delta = 0.1$ (circles), 0.05 (squares) and 0.025 (triangles).

TABLE I Variation of dissolution parameters with the proportion p_B of soluble species in glass for $\delta = 0.05$

p_B	0.00	0.10	0.15	0.20	0.25
$v_0(p_B)/v_0(p_B=0)$	1	7.2	29	170	1420
S_0/S	1.01	2.0	5.7	21	103
$\tilde{n}_0$	3.9	3.5	3.4	3.1	3.0

$v_0(p_B)/v_0(p_B=0)$ is the ratio of the rate of dissolution v_0 with respect to its value for a pure A system. S_0/S is the ratio of the stationnary area of the porous structure to the initial (flat) area of the interface and $\tilde{n}_0$ is the effective number of A neighbours for an A atom at the surface as defined by Equation 9.

where S_0 is the stationary surface area as obtained from Fig. 3. Equation 8 can be rewritten as:

$$v_0 = \frac{w_c}{p_A}\frac{S_0}{S}\tilde{n}_0 \delta^{\tilde{n}_0} \tag{9}$$

which defines $\tilde{n}_0$ as an effective number of A neighbours for an A atom at the surface. It should be noticed that $\tilde{n}_0$ as given by Equation 9 is different from the average number of neighbours (although they are expected to vary in the same way). Table I displays the variation with p_B of v_0, S_0/S and $\tilde{n}_0$ for $\delta = 0.05$ ($\tilde{n}_0$ is calculated from the data using Equation 9). It appears that v_0 increases by more than three orders of magnitude when p_B goes from 0 to 0.25 without changing the parameters for A dissolution. Meanwhile, S_0/S increases by two orders of magnitude and $\tilde{n}_0$ decreases from 3.9 to 3.0. The other simulations with $\delta = 0.025$ and $\delta = 0.1$ show that the increase of both the dissolution rate and the porous area is a bit weaker (stronger) when δ is larger (smaller). However, the values of $\tilde{n}_0$ are practically the same as in Table I (within less than ± 0.1) for the three values δ of we have investigated.

From Table I and Equation 9, we can understand the variation of the dissolution rate with the composition of the glass as resulting from two effects. First, increasing the proportion of the soluble B species results in a decrease of the mean coordination of the A species (reflected in the decrease of $\tilde{n}_0$ in Table I), which weakens the covalent network. Second, the fast leaching of the soluble species generates a porous structure which increases dramatically the surface offered for the dissolution of the A species (by a factor of 100 from $p_B = 0$ to $p_B = 0.25$). These two effects can be called chemical and structural, respectively. Although the first effect is more generally emphasized in the literature, the second one proves here to play the most important role in the increase of the dissolution rate with the proportion of soluble species.

6. Equilibrium solubility and saturation behaviour

Let us now describe the results of simulations with finite solution volume and recondensation of A species. Fig. 6 shows the evolution of a longitudinal cross-section for $p_B = 0.25$, $\delta = 0.05$ and $S/V = 4 \times 10^{-6}$. First, one observes the formation of a porous layer, whose growth stops after some time (about 5000 steps in the present case). Thereafter, there is a gradual rearrangement of the porous network with pore shapes becoming more

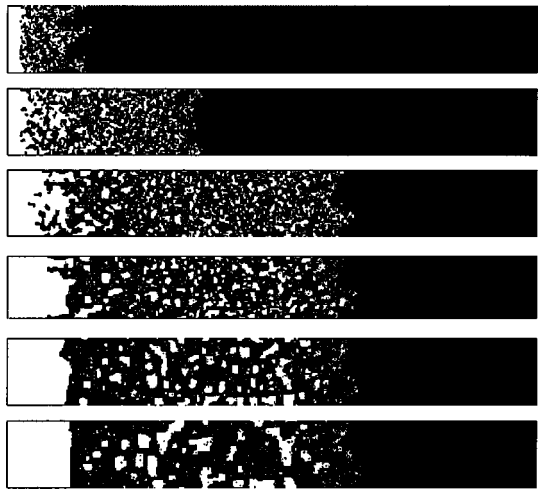

Figure 6 Evolution of a longitudinal cross-section (64×512) in a simulation with recondensation of A species. The parameters of the simulation are: $p_B = 0.25$, $w_h = 0.1$, $\delta = 0.05$ and $S/V = 4 \times 10^6$. Views at times $t = 10^3$, 3×10^3, 10^4, 3×10^4, 10^5 and 3×10^5.

regular and pore diameters larger. The porosity gets mostly occluded. The typical pore diameter in the aged sample is of the order of 5 to 10 sites, which corresponds to a few nm, in agreement with experimental observations [30]. This aging is related to the saturation of the solution in A species. When the saturation is reached, there are statistically as many dissolved A atoms as deposited ones in each computer step. However, according to Equations 3 and 4, A atoms are dissolved preferably from sites with a small number of neighbours and deposited onto those with a large number of neighbours. This generates a surface tension effect which is analogous to Ostwald ripening and tends to smooth the surfaces. One can also observe in Fig. 6 a slight shrinkage of the sample. In the present case, the shrinkage is quite limited because of the small solution volume and the weak solubility, but it may be much more important under other conditions. Fig. 7 shows the concentration profiles in the aged sample. It turns out that the porous layer is practically free of B atoms and that there is a sharp S-shaped transition in the B concentration at the interface between the porous layer and the unaltered glass. This is consistent with experimental results [14] and with the usual practice to monitor alteration by recording the release of boron and

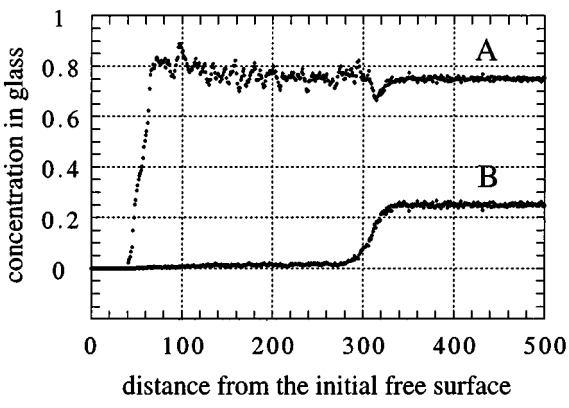

Figure 7 Concentration profiles in the aged porous layer ($t = 10^5$). The parameters of the simulation are the same as in Fig. 6.

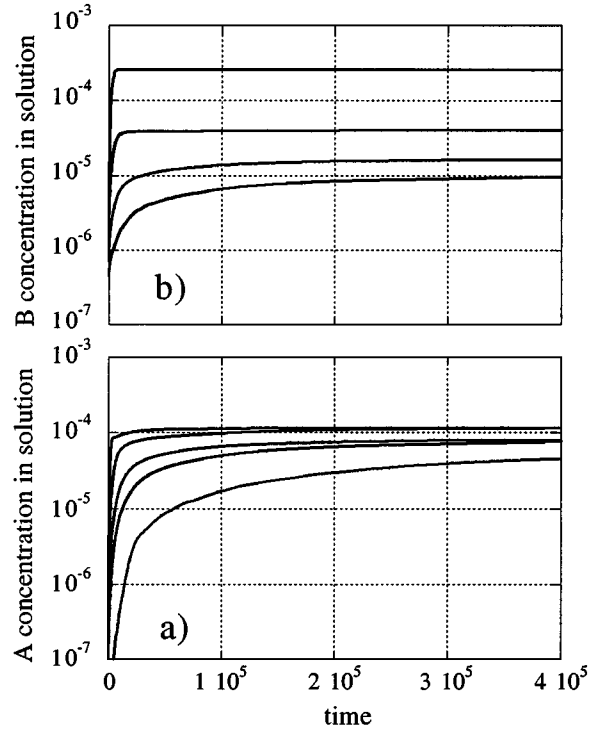

Figure 8 Variation with time of A and B concentrations in solution for $\delta = 0.05$ and $S/V = 4 \times 10^{-6}$. From bottom to top: $p_B = 0.0$ (for A only), 0.10, 0.15, 0.20 and 0.25.

alkalis in solution [11]. One also observes that the concentration of A atoms within the altered layer is nearly the same as in the pristine glass.

Fig. 8 displays the evolution of A and B concentrations in solution for $\delta = 0.05$ and p_B varying from 0 to 0.25. Though the time constants are strongly different from one curve to another, Fig. 8 shows that the A concentration saturates at values which are quite close to each other. The equilibrium A concentrations c_A^{eq} are given in Table II as a function of p_B and δ. They strongly depend on the hydrolysis-to-condensation ratio δ, but only slightly on the glass composition (less than a factor two when p_B is changed from 0 to 0.25). This is in sharp contrast to the enormous change in the initial dissolution rate (more than 1000 in Table I). The values of c_A^{eq} can be understood from Equation 5, which gives at equilibrium:

$$c_A^{eq} = \langle \delta^{n_i} \rangle_{i \in S_{eq}} = \delta^{\tilde{n}_{eq}} \qquad (10)$$

where the average is taken on the surface sites of the aged sample. It is not surprising that c_A^{eq} is found practically independent of p_B, since at long times all the B atoms have been removed from the porous layer. Thus, the mean environment of a surface A atom becomes the same in the aged interface, whatever is the initial composition. Equation 10 defines $\tilde{n}_{eq}$ as an effective number of A neighbours at equilibrium. Its value, as calculated from the concentrations in Table II, turns out to be independent of both p_B and δ and equal to 3.05 ± 0.05. This low value may seem in contradiction with the smooth surfaces of the aged sample. In fact, as previously mentionned in section 5 for $\tilde{n}_0$, $\tilde{n}_{eq}$ is not the mean number of neighbours of all the surface sites. It rather characterizes the sites which are predominantly active in the dissolution-condensation equilibrium. The

TABLE II A and B concentrations in saturated solution for different values of the parameters p_B and δ

p_B		0.00	0.10	0.15	0.20	0.25
$\delta = 0.025$	$10^5 c_A^{eq}$	0.8*	1.4	1.4	1.4	1.4
	$10^5 c_B^{lim}$	-	0.3	0.5	1.4	14.5
$\delta = 0.05$	$10^4 c_A^{eq}$	0.7*	0.8	0.9	1.2	1.2
	$10^4 c_B^{lim}$	-	0.11	0.18	0.42	2.9
$\delta = 0.1$	$10^3 c_A^{eq}$	0.7*	0.8	0.8	0.8	1.0
	$10^3 c_B^{lim}$	-	0.09	0.15	0.22	0.55

All the results have been obtained with $S/V = 4 \times 10^{-6}$. In some cases (*), the saturation is not completely reached at the longest time of the simulation.

sites with one or two neighbours, which are too weak, are immediately dissolved and the sites with four or five neighbours are too strong to be removed. Anyway, as changing δ by a factor of two changes the equilibrium A concentration by a factor of ten, one sees that a restricted range of δ values is sufficient to cover an extended range of solubility (the molar fraction range 10^{-5}–10^{-3} in Table II is equivalent to 0.55–55 m mol/l or 15–1500 mg/l of Si).

As observed for A species, the amount of dissolved B atoms also reaches a limit value c_B^{lim} (Fig. 8). However, the reason for it is different. For A species, the saturation results from the chemical equilibrium between dissolution and condensation reactions, while for B species, it is due to the occlusion of the porosity induced by the glass rearrangement. The departure of B species and the smoothing of the pore walls both contribute to make the aged sample more resistant than the initial glass. This prevents further extraction of B atoms beyond the porous layer. Unlike A, the B concentration limits given in Table II depend on both δ and p_B. This can be interpreted by considering the profile concentrations in the aged porous layer (Fig. 7). As the B concentration is almost zero and the A concentration is nearly the same as in the unaltered glass, one can write:

$$\begin{aligned} V c_A^{eq} &\equiv N_A^{eq} = p_A S d_s \\ V c_B^{lim} &\equiv N_B^{lim} = p_B S (d_s + e_g) \end{aligned} \tag{11}$$

where d_s and e_g are the shrinkage depth and the gel thickness, respectively. From Equation 11, it follows:

$$\frac{c_B^{lim}}{p_B} = \frac{c_A^{eq}(\delta)}{p_A} + \frac{S}{V} \times e_g(p_B) \tag{12}$$

where the dependence on the parameters, δ and p_B, has been explicitly emphasized. The first term in right-hand side of Equation 12 represents the congruent part of the dissolution. It mainly depends on the chemical parameter δ through the equilibrium concentration c_A^{eq}. The second term, which is the incongruent part, is proportional to the glass surface area to solution volume ratio and to the gel thickness. Fig. 9 shows that the latter is fully determined by the glass composition. It goes from a few atomic layers for $p_B = 0$ to about 300 atomic layers (~100 nm) for $p_B = 0.25$. These two values are consistent with the experimental observations for the glasses of types I and II in the classification by Hench and Clark [5].

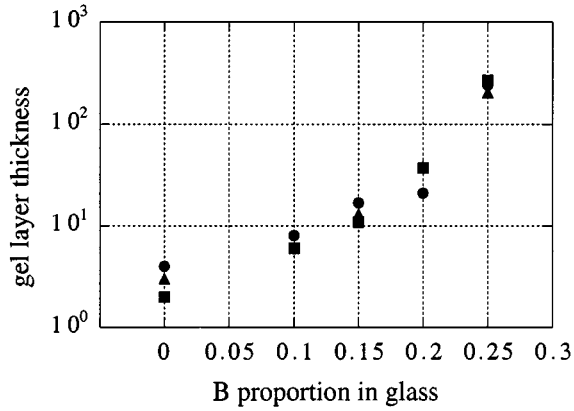

Figure 9 Variation of the thickness of the gel layer e_g for $S/V = t \times 10^{-6}$ as a function of the proportion p_B of soluble species in glass for $\delta = 0.1$ (circles), 0.05 (squares) and 0.025 (triangles).

An immediate consequence of Equation 12 is the breaking of the $(S/V) \times t$ scaling in the saturation regime. To bring this effect into prominence, simulations with different S/V ratio have been performed for $p_B = 0.25$ and $\delta = 0.05$. The main results are summarized in Table III. Experimentally, the values chosen for S/V would correspond to about 2×10^2, 2×10^3, 2×10^4 and 2×10^5 m^{-1}. One sees that the A concentration at saturation is nearly independent of S/V, implying that the scaling is almost obeyed, as far as A species are concerned. This is not the case for the B species whose limit concentration increases plainly with S/V. This increase is weaker than the linear variation predicted by Equation 12, because at the same time the thickness of the altered layer is a decreasing function of S/V. Table III also gives the variation of the congruence ratio. It can be expressed from Equation 12 as:

$$\rho \equiv \frac{c_B^{lim} / p_B}{c_A^{eq} / p_A} = 1 + p_A \frac{S}{V} \frac{e_g(p_B, S/V)}{c_A^{eq}(\delta)} \tag{13}$$

When S/V goes to zero, one expects to recover the congruent dissolution evidenced in Section 5. Both the breaking of the $(S/V) \times t$ scaling and the departure from congruent dissolution are generally observed in experiments at high S/V [17, 20]. They appear here to result from the extraction of boron and alkalis from the gel layer, whose relative weight in the whole dissolution increases with S/V. To our knowledge, this is the first time that a simple explanation is provided for these observations.

7. Effect of less soluble species

One introduces now a new C species in order to represent less soluble oxides such as Al_2O_3, ZrO_2,

TABLE III Altered layer thickness, A and B concentrations in saturated solution and congruence ratio for different S/V ratio

S/V	4×10^{-8}	4×10^{-7}	4×10^{-6}	4×10^{-5}
e_g	850	440	300	160
$10^4 c_A^{eq}$	0.9	1.05	1.2	1.2
$10^4 c_B^{lim}$	0.36	0.72	2.9	15
ρ	1.2	2.1	7.3	37

The simulations have been made with $\delta = 0.05$ and $p_B = 0.25$.

Fe_2O_3, ... C species are expected to have a low solubility and to form more resistant bonds. To take into account these new species, Equations 3 and 4 are generalized by defining hydrolysis (w_h) and condensation (w_c) rate constants for A-A, A-C and C-C bonds. Within the same assumptions as in Section 4, it is easy to show that the dissolution rate constants for A and C atoms depend on their numbers of A and C neighbours (n_i^A and n_i^C) as:

$$w_d^A(i) = \left(n_i^A w_c^{AA} + n_i^C w_c^{AC}\right)\left(\frac{w_h^{AA}}{w_c^{AA}}\right)^{n_i^A}\left(\frac{w_h^{AC}}{w_c^{AC}}\right)^{n_i^C} \tag{14}$$

$$w_d^C(i) = \left(n_i^A w_c^{AC} + n_i^C w_c^{CC}\right)\left(\frac{w_h^{AC}}{w_c^{AC}}\right)^{n_i^A}\left(\frac{w_h^{CC}}{w_c^{CC}}\right)^{n_i^C}$$

while the depositing rate constants are expressed as:

$$\begin{aligned} w_r^A(i) &= \left(n_i^A w_c^{AA} + n_i^C w_c^{AC}\right)c_A \\ w_r^C(i) &= \left(n_i^A w_c^{AC} + n_i^C w_c^{CC}\right)c_C \end{aligned} \tag{15}$$

where c_C is the concentration of C atoms in solution.

The presence of A-C and C-C bonds introduces four new parameters, for which the choice of values is somehow arbitrary. We have taken: $w_h^{AA} = w_h^{AC} = w_h^{CC} = 0.1$, $w_c^{AA} = 2$ and $w_c^{AC} = w_c^{CC} = 20$, so that the hydrolysis and the condensation of A-A bonds remain the same as before (in the case $\delta = 0.05$) and the condensation of A-C and C-C bonds is ten time faster than that of A-A bonds. This choice is consistent with the idea that cations such as Al or Zr are much more reactive than silicon, although they are less soluble. Simulations have been carried out for $p_B = 0.25$ and two values of the concentration of C species: $p_C = 0.05$ and 0.10.

The main results are given in Table IV. One observes that the presence of C species depresses the initial rate of dissolution and more significantly the A concentration at saturation. However, the limit B concentration increases slightly, whereas the C concentration remains extremely small. From Equations 14 and 15, the equilibrium of the dissolution and condensation fluxes gives:

$$\begin{aligned} c_A^{eq} &= (\delta_{AA})^{\tilde{n}_A^{eq}}(\delta_{AC})^{\tilde{n}_C^{eq}} \\ c_C^{eq} &= (\delta_{AC})^{\tilde{n}_A^{eq}}(\delta_{CC})^{\tilde{n}_C^{eq}} \end{aligned} \tag{16}$$

where $\tilde{n}_A^{eq}$ and $\tilde{n}_C^{eq}$ are the effective numbers of A and C neighbours of a surface atom in the aged interface, and δ_{AA}, δ_{AC} and δ_{CC} are the ratio of hydrolysis to condensation rates for A-A, A-C and C-C bonds, respectively.

TABLE IV Dissolution rate and A, B and C concentrations in saturated solution as a function of p_C

p_C	0	0.05	0.10
$v_0(p_C)/v_0(p_C=0)$	1	0.77	0.61
$10^4 c_A^{eq}$	1.2	0.4	0.2
$10^4 c_B^{lim}$	2.9	3.6	4.1
$10^8 c_C^{eq}$	-	1.0	2.0

The dissolution rate is referred to its value for $p_C = 0$. The simulations have been made with $\delta_{AA} = 0.05$, $\delta_{AC} = \delta_{CC} = 0.005$ and $p_B = 0.25$. The concentrations at saturation are obtained for $S/V = 4 \times 10^{-6}$.

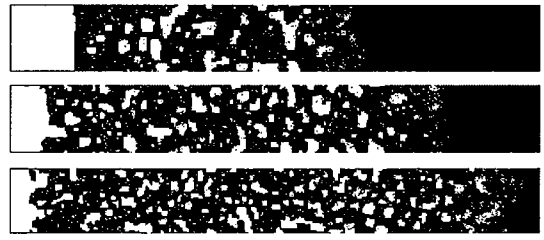

Figure 10 Comparison of longitudinal cross-sections (64 × 512) of aged interfaces ($t = 3 \times 10^5$) for $p_C = 0.0$, 0.05 and 0.10 (from top to bottom). The parameters of the simulations are: $p_B = 0.25$, $\delta_{AA} = 0.05$, $\delta_{AC} = \delta_{CC} = 0.005$ and $S/V = 4 \times 10^{-6}$.

The decrease of c_A^{eq} and the low value of c_C^{eq} result directly from the existence of the stronger A-C and C-C bonds with $\delta_{AC} = \delta_{CC} < \delta_{AA}$.

Fig. 10 shows pictures of the aged porous layer for $p_C = 0.00$, 0.05 and 0.10. The presence of C has three consequences on the layer morphology. First, the final thickness of the porous layer is larger, secondly, the shrinkage has been practically suppressed and thirdly the ripening effect is less important, which results in smaller pore sizes. All these effects are related to the fact that C atoms are almost insoluble. Their presence pins down hard clusters around which the glass should rearrange. This inhibits the large scale restructuration observed in AB systems. The increase of the amount of dissolved B species in presence of quasi-insoluble species (Table IV) is a direct consequence of the larger penetration depth. Therefore the presence of C species decreases the solubility of A species, but increases that of B species. This paradoxical result is unexpected and will be discussed in the next section.

8. Discussion

In this section, we would like to discuss the relevance of our model for glass dissolution. It is quite certain that such a simplified model cannot quantitatively reproduce the experiments on complex real glasses. Its ambition is rather to provide an heuristic tool to improve the understanding of glass dissolution and to emphasize qualitative behaviours and trends. In this respect, we believe that it captures a number of major features of the dissolution of durable glasses in the neutral to moderate basic conditions. Among these features, one can mention (i) the very large range of dissolution rates [2, 18] associated to a much more limited range of solubility in silica [2], (ii) the existence of a dealkalized hydrated porous layer whose thickness increases sharply with the alkali content [5] and decreases with the S/V ratio [25], (iii) the stationary congruent dissolution following an initial phase of selective extraction of soluble species [22, 25], (iv) the departure from congruence and the breaking of the $(S/V) \times t$ scaling at high S/V ratio for boron and alkalis extraction [15, 20, 25] and (v) the large rearrangement of the surface layer in the absence of insoluble oxides contrasted to the more limited rearrangement when they are present [2]. This overall agreement seems to imply that interdiffusion, which has been neglected here, plays only a secondary role, at least in the main phase of the dissolution process.

Of course, the consideration of only three species to represent the large number of oxides which may enter

in the composition of the real glasses, and especially in that of the nuclear waste glasses, is an oversimplification. For example, it is known that the behavior of heavy alkalis may be different from that of light alkalis, although both are well soluble in water. This is also true for the alkaline earths. As mentionned in Section 2, the alkali and alkaline earth oxides should be considered as less soluble C species, when their cations act as compensators of the excess negative charges of 4-coordinated Al or 6-coordinated Zr. However, in the case of alkaline earths, the situation is probably more complicated, since they seem to play a role by themselves in the durability of glasses. They are less soluble than alkalis and they may form redeposition barriers at the glass surface. As regards the insoluble or quasi-insoluble oxides, some of them (ZrO_2 or Al_2O_3) are much more efficient than others (Fe_2O_3 or TiO_2) in reinforcing the glass against leaching. As a rule, there is no objection to take into account new species with more varied behaviours in the simulations. However, this would imply to introduce an increasingly large number of parameters to describe the binary interactions between all the considered species. This seems to be untimely at the present stage of development of the model.

In the attempt to correlate the durability of glasses with their composition, our model appears complementary of that based on the free energy of hydration [4, 9]. The latter is able to sort out the glasses by computing a macroscopic energy of hydration as a weighted average of the energies of hydration of their components. By considering only three classes, our model is much rougher in this respect. The assumption of unconditionnal dissolution of the soluble B species is equivalent to an infinitely negative free energy of hydration for these species. On the other hand, since our simulations handle the particles individually, they provide a microscopic picture of the glass corrosion and they make it possible to predict the selective release of the different glass components in solution. Moreover, the model supplies information on the morphology of the altered layer and on the kinetics of the leaching.

In the field of nuclear glasses, there is a dispute to know whether the slowing down of the corrosion at long time is due to the saturation of the solution or to the protective nature of the surface layer [8, 26]. We believe that this is a biased question, because the protective effect of the layer results from the aging, which follows the saturation. However, saturation by itself is not sufficient. As a matter of fact, the dissolution-recondensation of silica is a dynamical equilibrium. Even long after the solution saturation is reached, there are always silicon species which are removed somewhere to be deposited again elsewhere. This process exposes new soluble species, which should be extracted from the glass at a rate basically controlled by the silica primary (not compensated) dissolution rate. This mechanism gives rise to dynamical percolation (in opposition to static percolation which takes place when the concentration of soluble species is above the percolation threshold). To avoid percolation or, at least, to significantly slow down the advance of the leaching front, the alkalis should become less accessible. This requires the reinforcement of the glass in the surface layer, which is well demonstrated in our simulation results when surface tension is included.

Experimentally, the long-time extraction rate of boron and alkalis, as obtained in static tests, is considerably reduced with respect to the initial rate (by three to four orders of magnitude), but generally it does not vanish [17, 22, 25]. Although the question is of paramount importance for the long-term behaviour of nuclear waste glasses, the origin of this residual alteration remains unclear [25]. Several mechanisms have been evoked, among which the interdiffusion of alkalis and water [40], the slow drift of the solution pH which may be complicated by local effects in the surface region, the deposition of secondary phases which may maintain out-of-equilibrium the glass-solution reaction [16] and the formation of cracks resulting from the stresses accumulated in the hydration layer. This latter point is of special importance, since it can induce a renewal of the alteration after a period of time corresponding to the advent of cracking. As this interval of time is expected to depend on the glass composition, this may be at the origin of the difference between the so-called durable and less durable glasses in short time alteration tests. To check these different hypotheses, it would be interesting to perform experimental studies in conditions where some of these effects are inhibited, for example, leaching in controlled pH conditions or alteration of simplified glasses designed to be free of the cations involved in secondary phases.

As seen in Section 6, our simulations predict a complete freezing of the glass corrosion after the saturation of the solution in silica. There are *a priori* two ways to recover a (slow) progression of the leaching process. The first one, which can be considered as extrinsic, would consist of taking into account interdiffusion or introducing a drift in silica solubilitity resulting either from a pH shift or from the deposition of the secondary phases. The second way, which is more intrinsic, is to modify the model in order to reduce the layer rearrangement. As a matter of fact, it is likely that the present results overestimate this rearrangement. This comes basically from the fact that our simulations do not deal actually with a glass. When B species have been removed in an AB system, the porous layer tends to rearrange as a single A crystal. This explains the paradoxical role of C species mentionned in Section 7. Although they depress the dissolution rate and the silica solubity, they act as defects, which restrain the large scale rearrangement. This delays somewhat the porosity occlusion and leads to a (slight) increase of the alteration depth.

Our results open the question of the existence of occluded porosity in the alteration layer. Although there is currently no definite experimental answer to this question, we prefer to assume for the present time that this is an artefact of the calculation. To avoid this effect, it is necessary to maintain the porous layer out-of-equilibrium. A possible way to reach this end is to introduce kinetic barriers for large scale rearrangement or random distributions of bond energies for representing steric hindrance to bond formation. Also, it may be better to inhibit the deposition of A atoms on some sites, for

example those previously occupied by small alkalis, to account for the local rearrangement which may immediately follow the departure of these atoms. A few trial simulations have been performed in these directions. In some cases, one observes from time to time bursts of porosity reopening. These rare events could provide a way to recover a residual leaching at long time.

9. Conclusion

Our model for glass dissolution basically rests on two parameters, the proportion of soluble species, which caracterizes the glass composition, and the hydrolysis-to-condensation ratio of the network-former species, which describes the chemistry of the glass-water system. The latter is modified by the presence of insoluble oxides, but it also depends on the external conditions such as temperature or pH. Our principal results concern the structure of the porous layer, the rate of dissolution and the equilibrium solubility. The thickness of the porous layer is mainly controlled by the proportion of soluble species in the glass. In turn, this governs the rate of dissolution in dynamic conditions and the total amount of soluble species extracted from the glass in static conditions. On the contrary, the solubility of the glass-former species is mostly determined by the hydrolysis-to-condensation ratio, since it results from a local (dynamic) equilibrium and does not depend in first approximation on the interface morphology. The most important issue is the freezing of the leaching, which results from the restructuration of the altered layer, when surface tension is included in the model. This provides a simple explanation for the protective role of the surface layer, which have been demonstrated in the recent experimental studies [26, 31, 41]. Further work is required to describe accurately the residual slow progression of the glass corrosion which is experimentally observed in long-term static tests.

Acknowledgment

This work is partly supported by the Commisariat à l'Energie Atomique (contract CEA/SCD n° B98/260). We thanks Jean-Marc Delaye, Stephane Gin, Yves Minet and Etienne Vernaz for comments and fruitful discussions and Laure-Amélie Couturier and Jeannette Lepage for invaluable technical support. Finally, we are indebted to the anonymous referree for his (her) suggestions of improvement concerning both the style and the scientific content.

References

1. R. K. ILER, "The Chemistry of Silica" (Wiley, New York, 1979) Ch. 1.
2. R. H. DOREMUS, "Glass Science" 2nd ed. (Wiley, New York, 1994) Ch. 13.
3. Z. BOKSAY, G. BOUQUET and S. DOBOS, *Phys. Chem. Glasses* **9** (1968) 69.
4. A. PAUL, *J. Mater. Sci*. **12** (1977) 2246.
5. L. L. HENCH and D. E. CLARK, *J. Non-Cryst. Solids* **28** (1978) 83.
6. H. SCHOLZE, *ibid.* **52** (1982) 91.
7. B. M. J. SMETS and T. P. A. LOMMEN, *Phys. Chem. Glasses* **23** (1982) 83.
8. L. A. CHICK and L. R. PEDERSON, *Mat. Res. Symp. Proc*. **26** (1984) 635.
9. C. M. JANTZEN and M. J. PLODINEC, *J. Non-Cryst. Solids* **67** (1984) 207.
10. B. GRAMBOW, *Mat. Res. Symp. Proc*. **44** (1985) 15.
11. B. E. SHEETZ, W. P. FREEBORN, D. K. SMITH, C. ANDERSON, M. ZOLENSKY and W. B. WHITE, *ibid*. **44** (1985) 129.
12. B. C. BUNKER, G. W. ARNOLD, D. E. DAY and P. J. BRAY, *J. Non-Cryst. Solids* **87** (1986) 226.
13. B. C. BUNKER, D. R. TALLANT, T. J. HEADLEY, G. L. TURNER and R. J. KIRKPATRICK, *Phys. Chem. Glasses* **29** (1988) 106.
14. H. SCHOLZE, *J. Non-Cryst. Solids* **102** (1988) 1.
15. X. FENG, I. L. PEGG, A. BARKATT, P. B. MACEDO, S. J. CUCINELLI and S. LAI, *Nucl. Tech*. **85** (1989) 334.
16. W. L. BOURCIER, D. W. PEIFFER, K. G. KNAUSS, K. D. MCKEEGAN and D. K. SMITH, *Mat. Res. Symp. Proc*. **176** (1990) 209.
17. X. FENG, I. L. PEGG, Y. GUO, A. A. BARKATT and P. C. MACEBO, *ibid*. **176** (1990) 383.
18. G. PERERA and R. H. DOREMUS, *J. Amer. Ceram. Soc*. **74** (1991) 1269.
19. M. KINOSHITA, M. HARADA, Y. SATO and Y. HARIGUCHI, *ibid*. **74** (1991) 783.
20. T. ADVOCAT, PhD thesis, Université Louis Pasteur, Strasbourg, France, 1991.
21. T. ADVOCAT, J. L. CROVISIER, E. Y. VERNAZ, G. EHRET and G. CHARPENTIER, *Mat. Res. Soc. Symp. Proc*. **212** (1991) 57.
22. E. VERNAZ and J. L. DUCHAUSSOY, *Appl. Geochem.* **1** (1992) 13.
23. S. B. XING, I. S. MULLER and I. L. PEGG, *Mat. Res. Symp. Proc*. **333** (1994) 549.
24. S. B. XING, PhD thesis, The Catholic university of America, Washington DC, USA, 1994.
25. W. L. EBERT and J. J. MAZER, *Mat. Res. Symp. Proc*. **333** (1994) 27.
26. S. B. XING, A. C. BUECHELE and I. L. PEGG, *ibid*. **333** (1994) 541.
27. M. AERTSENS and P. VAN ISEGHEM, *ibid*. **412** (1996) 271.
28. C. JEGOU, PhD thesis Université du Languedoc, Montpellier, France, 1998.
29. M. AERTSENS, *Mat. Res. Symp. Proc*. **556** (1999) 409.
30. O. DERUELLE, O. SPALLA, PH. BARBOUX and J. LAMBARD, *J. Non-Cryst. Solids* **241** (2000) 237.
31. C. JEGOU, S. GIN and F. LARCHÉ, *J. Nucl. Mat*. **280** (2000) 216.
32. F. DEVREUX and M. KOLB, *J. Non-Cryst. Solids* **242** (1998) 14.
33. S. B. SANTRA, B. SAPOVAL, PH. BARBOUX and F. DEVREUX, *C.R. Acad. Sci (Paris)* **326** (1998) 129.
34. P. MEAKIN, T. JOSSANG and J. FEDER, *Phys. Rev. E* **48** (1993) 2906.
35. A. HERNANDEZ-CREUS, P. CARRO, R. C. SALVAREZZA and A. J. ARVIA, *J. Electrochem. Soc*. **142** (1995) 3806.
36. B. SAPOVAL, S. B. SANTRA and PH. BARBOUX, *Europhys. Lett*. **41** (1998) 297.
37. D. STAUFFER, "Introduction to Percolation Theory" (Taylor & Francis, London, 1985).
38. M. LOBANOVA, L. MAURER, PH. BARBOUX, F. DEVREUX and Y. MINET, Communication to the 24th Symposium on The Scientific Basis for Nuclear Waste Management (Sydney, Australia, 28–31 August 2000), *Mat. Res. Symp. Proc*, to appear.
39. J. HOSCHEN and R. KOPELMAN, *Phys. Rev B* **14** (1976) 3428.
40. B. GRAMBOW, Communication to The International Workshop on Glass in its Disposal Environment (Bruges, Belgium, 11–14 April 2000) *J. Nucl. Mat*, to appear.
41. S. GIN and E. VERNAZ, Communication to the 24th Symposium on The Scientific Basis for Nuclear Waste Management (Sydney, Australia, 28–31 August 2000), *Mat. Res. Symp. Proc*, to appear.

Received 5 May
and accepted 16 October 2000